Heliyon 6 (2020) e03546

Contents lists available at ScienceDirect

Heliyon

journal homepage: www.cell.com/heliyon

Research article

SEM, XRD and FTIR analyses of both ultrasonic and heat generated activated carbon black microstructures

Pratama Jujur Wibawa [a,b,*], Muhammad Nur [b], Mukhamad Asy'ari [a], Hadi Nur [c]

[a] Department of Chemistry, Faculty of Sciences and Mathematics Diponegoro University, Jalan Prof. H. Soedarto, SH. No.1 Tembalang, Semarang, Indonesia
[b] Center for Plasma Research, Department of Physics, Faculty of Sciences and Mathematics Diponegoro University, Jalan Prof. H. Soedarto, SH. No.1 Tembalang, Semarang, Indonesia
[c] Center for Sustainable Nanomaterials, Ibnu Sina Institute for Scientific and Industrial Research, Universiti Teknologi Malaysia, 81310, Skudai, Johor, Malaysia

ARTICLE INFO

Keywords:
Micromaterials
SEM analysis
XRD Analysis
Activated carbon black microparticles
FTIR analysis
Ultrasonic treatment

ABSTRACT

The microstructures of the activated carbon black microparticles (ACBMPs) generated through both treatments of 20 min ultrasonic and 400 °C thermal energy equivalent have been analyzed properly using scanning electron microscope (SEM), X-ray diffraction (XRD) and Fourier-transformed infrared (FTIR) spectroscopy methods. The research was aiming to generate binding or active sites points on the outer surface of the ACBMPs body of which commonly plays an important role in both adsorption and catalytic processes. It was observed that around 150 nm up to 400 nm in average diameter super macro voids with many various turns of nano-scale wells, and around 1.84 angstrom (Å) up to 15.98 Å intraparticle pores were generated. In addition, the parallel planes spacing of the carbonaceous framework sheets, namely d_{hkl} in Miller indexes terminology, of about 4.44 Å up to 2.98 Å constructed the inner particles of the ACBMPs body. A new nomenclature method for the binding or active site shapes identification and classifying them into four categories based on the quadrants terminology, *i.e.* quadrant one (Q1), two (Q2), three (Q3) and four (Q4) is proposed. Each the quadrants contains four categories of turns types, *i.e.* sharp, semi sharp, obtuse and non-significant turns depending on the angle of the associated turn in radian angle, θ. Finally, it can be concluded that the combination of ultrasonic and thermal energy treatments in fabricating ACBMPs could generate binding or active site points with unique shapes as a transit terminal for any guest molecules, in this context is methyl red (MR) molecules to enter into the suitable intra-particles pores of the ACBMPs body.

1. Introduction

Activated carbon black (ACB) is the most popular ancient porous materials with a large internal surface area ranging from 500 to 2000 m^2g^{-1} (Suhas et al., 2007) that has been widely used for various applications, particularly in both powerful adsorbent (Jutakridsada et al., 2016; Veksha et al., 2016; Shafeeyan et al., 2010) and catalyst (Show and Ueno, 2017; Suryanto and Zhao, 2016; Sairanen, 2015) manufacturing. Referring (Suhas et al., 2007) the ACB can be available in two main forms, namely powder activated carbon black (PACB) and granular activated carbon black (GACB). The difference between PACB from GACB is exactly confirmed by their particles size. The particles sizes of PACB are less than 0.2 mm in diameter so that it has large external surface area and small diffusion resistance, while that of the GACB are about more than 5 mm in diameter so that it has smaller external surface area. This particles difference leads to the difference in their applications. For example, GACB is commonly preferred to be applied for gases and vapors adsorption processes and fixed bed filtration systems due to its easier regeneration than that of PACB (Suhas et al., 2007). Accordingly, the size of ACB particles is an important key to provide useful properties of the ACB-based materials. In relation to that, reducing the size of the ACB particles from bigger to smaller one even up to nano-scale in particles size and exploring their adsorption capability in relation with their nanostructures is necessary to be conducted. This information is required not only for the development of advanced and smart carbon-based materials including super catalyst and high-performance adsorbent fabrications but also for the determination of the relationship of the generated microstructures types with their adsorption and catalytic properties. In correlation to that, it has widely well known that shape, size and surface morphology of any material of nano-scale in size are exactly determining

* Corresponding author.
E-mail address: pratamajw@live.undip.ac.id (P.J. Wibawa).

https://doi.org/10.1016/j.heliyon.2020.e03546
Received 4 June 2018; Received in revised form 10 December 2018; Accepted 2 March 2020

factors of the nano-scale size materials properties rather than its chemicals structures (Narayanan et al., 2018; Nallusamy et al., 2017a; Nallusamy et al., 2017b; Nallusamy, 2016). Thus, the nomenclature method of the generated microstructure based on its shape is very important to be formulated. However, almost all the generated microstructures of the ACB materials and their derivates ones fabricated through pyrolysis process and activated with chemical as well as physical activation, including use thermal energy are still not have a name. In other word, until this moment all the microstructures of the ACB-based materials have not named yet. This situation causes to the theory of the micro/-nanomaterials identification as well as whatever related to it has not developed completely at this time. Therefore, the nomenclature method of the ACB materials microstructure generated by thermal energy and ultrasound treatment is described comprehensively in this paper.

Accordingly, this paper describes the fabrication of ACB microparticles by pyrolysis and ultrasonic agitation to generate the microstructure of ACB-based materials; the scanning electron microscope (SEM), X-ray diffraction (XRD) and Fourier-transformed infrared (FTIR) spectroscopy analyses of the generated microstructures; the inter ACB particles pores modeling; the nomenclature method of the generated microstructures based on their pores shape and finally the conclusion remark.

2. Experimental sections

Materials: Local commercial Carbon black, local commercial Virgin coconut oil (VCO), local commercial Distilled water (DW), Phosphoric acid (H_3PO_4) p.a; Sodium hydroxide (NaOH) p.a. Methyl red dyes, p. a. Whatman filter paper of grade 1. All the chemicals were produced by Sigma-Aldrich, Germany.

Equipments: Commonly used laboratory glassware tools, Electrical Oven (Cosmos CO-9919 Indonesia), Furnace (Vulcan 3-130, USA), Ultrasonic cleaner set (Krisbow CD4862, China), pH meter (Senz pH Scientific Trans Instrument, Singapore), Analytical Scanning Electron Microscope-Energy Dispersive X-ray (SEM-EDX, JEOL JSM-6510LA, Japan), Particles Size Analyzer (PSA) (Horiba Scientific SZ-100, USA), X-ray Diffractometer (XRD6100 Shimadzu, Japan), Fourier-Transform Infrared Spectrometer (FTIR Perkin Elmer, USA). UV-Vis spectrometer (UV-1280, Shimadzu, Japan).

2.1. Fabrications of activated carbon black microparticles of ACBMPs code

It was started by milling of 200 g commercial carbon black (CB) powder into 100 meshes (80 microns) using a ball milling machine. This fine CB powder was then mixed properly with 1000 mL DW/VCO (995:5 in volume ratio), treated with ultrasonic (US) agitation (40 kHz, 2 × 50 W) for 20 min and let it to equilibrate at room temperature for about 24 h. The aqueous phase of upper layer was removed out from the mixture by decantation method to obtain CB of micro-scale size, which was then encoded as CBMPs. The sample of CBMPs was then dried at 110 °C in an electrical oven until constant weight was reached. Furthermore, the dried CBMPs was then activated according to the following procedure, and the obtained activated carbon black microparticle was encoded as ACBMPs. The following is the activation procedure for the ACBMPs material fabrication. Three samples consisted of about 50 g CBMPs each was homogenously mixed with 50, 75 and 100 g H_3PO_4 to obtain 1:1; 1:1.5; 1:2 mass ratios as performed by Gratuito et al. (2008) and later encoded as ACBMPs. These samples were then incubated at a room temperature for about 12 h. After that, every 2.5 g of the ACBMPs samples were heated in a furnace at various temperatures and time, *i.e.* 400 °C, 500 °C and 600 °C for 20, 40 and 60 min each.

Furthermore, all samples were then washed thoroughly several times with distilled water until pH about 7 then by 0.5 M NaOH solution until the remaining acid was removed out. Finally, the samples were then washed again by distilled water until pH 7 was exactly reached, dried-up them in an electrical oven at 105 °C. After that, the fabricated ACBMPs samples were analyzed deeply employing SEM, XRD and FTIR spectrometers. The analyses were focused on their surface morphology pattern to explore the generated inter particles pore shape of the associated ACBMPs material, basal spacing and typical chemical bonds vibration to identify the graphene-like structure.

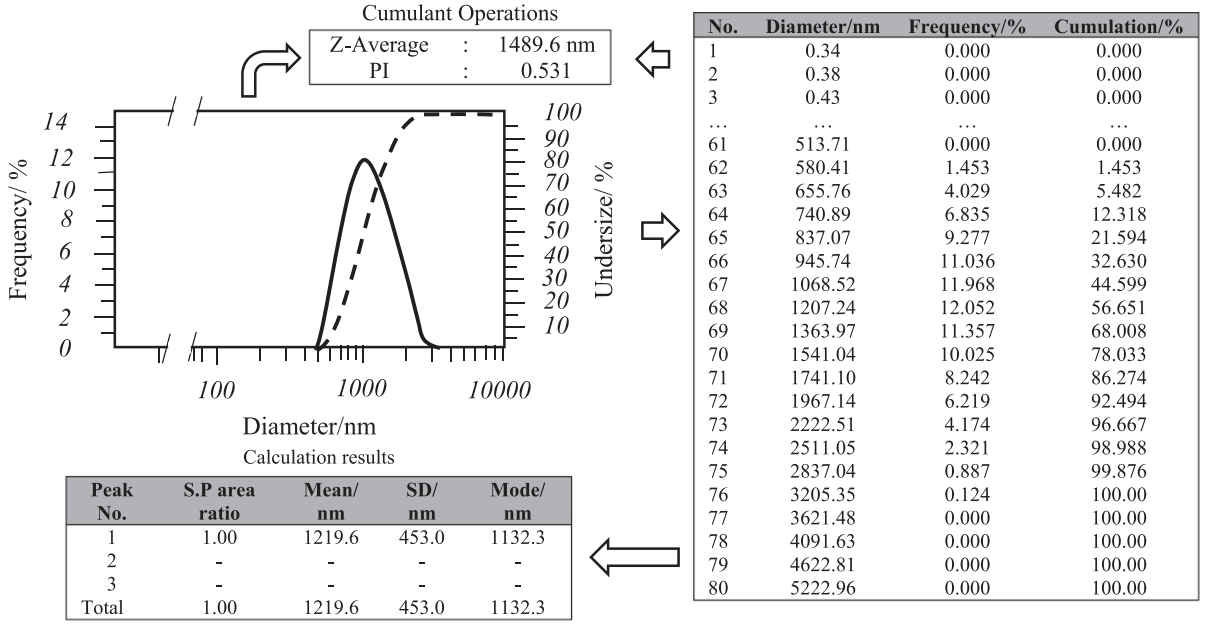

Peak No.	S.P area ratio	Mean/ nm	SD/ nm	Mode/ nm
1	1.00	1219.6	453.0	1132.3
2	-	-	-	-
3	-	-	-	-
Total	1.00	1219.6	453.0	1132.3

No.	Diameter/nm	Frequency/%	Cumulation/%
1	0.34	0.000	0.000
2	0.38	0.000	0.000
3	0.43	0.000	0.000
…	…	…	…
61	513.71	0.000	0.000
62	580.41	1.453	1.453
63	655.76	4.029	5.482
64	740.89	6.835	12.318
65	837.07	9.277	21.594
66	945.74	11.036	32.630
67	1068.52	11.968	44.599
68	1207.24	12.052	56.651
69	1363.97	11.357	68.008
70	1541.04	10.025	78.033
71	1741.10	8.242	86.274
72	1967.14	6.219	92.494
73	2222.51	4.174	96.667
74	2511.05	2.321	98.988
75	2837.04	0.887	99.876
76	3205.35	0.124	100.00
77	3621.48	0.000	100.00
78	4091.63	0.000	100.00
79	4622.81	0.000	100.00
80	5222.96	0.000	100.00

Figure 1. The graph of the ACBMPs particles size analysis.

2.2. Characterization and analysis

2.2.1. Particles size analysis

The first characterization performed was the determination of the fabricated ACBMPs particles size using a PSA analytical instrument (Horiba Scientific SZ-100, USA) based on dynamic light scattering (DLS) method. The widely used parameters to measure the particles size in its dispersion system were applied by Mailer et al. (2015) and Hallett (1994). In this method, the hydrodynamic diameter (D_h) of the fabricated ACBMPs particles was expressed as $D_h = (k_B T)/(3\pi\eta D_t)$ namely Stokes-Einstein equation, where k_B, T, η and D_t each is Boltzman constant, temperature of the measurement in Kelvin, dynamic viscosity and the diffusion coefficient of translational particles motions respectively. In this correlation, $D_t = -\ln C/[2(4\pi n/\lambda)^2 \mathrm{Sin}^2(\theta/2)]$ where C, n, λ and θ each is the baseline subtracted ACF (autocorrelation function versus delay time in μsec), refractive index of the liquid medium, laser light wavelength beam and the laser light scattering angle respectively (Horiba, 2014). Here the primary result of the particles sizes population was statistically expressed as mean value derived from both intensity distribution of the scattered light called as the Z-average and polydispersity index (PI) of the measured particles.

2.2.2. Surface morphology analysis by SEM

Surface morphology images of the ACBMPs materials were characterized by SEM instrument (SEM-EDX, JEOL JSM-6510LA, Japan). The instrument was operated on the default parameters that commonly used to scan the surface morphology of samples for the best images with various magnifications of 5,000; 10,000 and 20,000 times. The SEM parameters employed in this research were adopted from Wibawa et al. (2011) with suitable matching.

2.2.3. The parallel planes distance (d-spacing) analysis by XRD spectroscopy

Crystanility and distance of the parallel plane (*d*-spacing) of the ACBMPs materials was determined by XRD (XRD6100 Shimadzu, Japan)

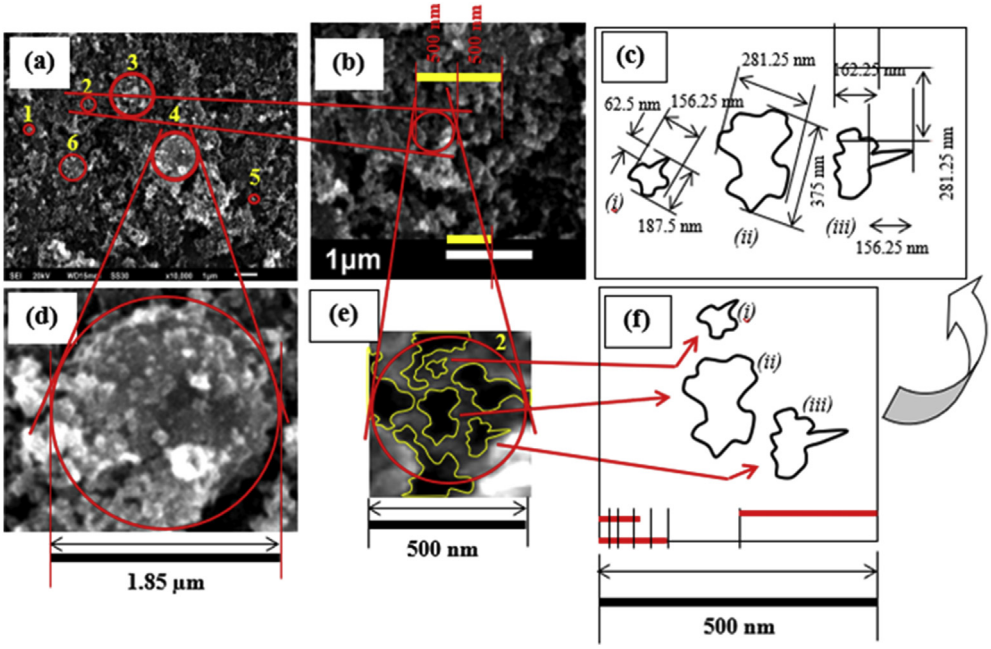

Figure 2. (a)SEM image of ACBMPs materials surface morphology with 6 areas of 1–6, 10,000 x magnification; (b) The 2 × 400% enlargement zoom of SEM image, area 2; (c) Schematic duplication of the surface of ACBMPs particles pores including the pores size dimension; (d) The 2 × 400% enlargement zoom of SEM image, area 4; (e) The 7 × 400% enlargement zoom of SEM image, area 2; (f) Various forms duplicates of ACBMPs materials pores.

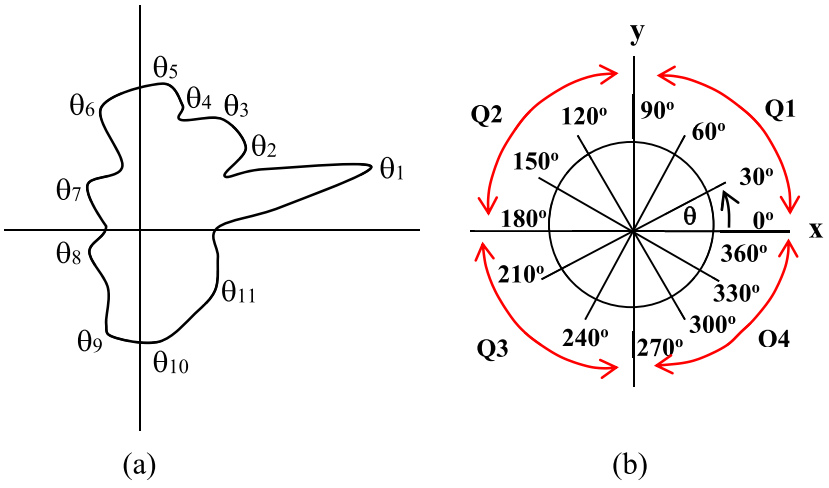

Figure 3. A guidance of the turn's nomenclature of carbon black-based pore surface, (a) The enlarged pore surface representative of ACBMPs materials, mark *(iii)* shown in Figure 2c, f; (b) Map of quadrant-based angles in radian unit.

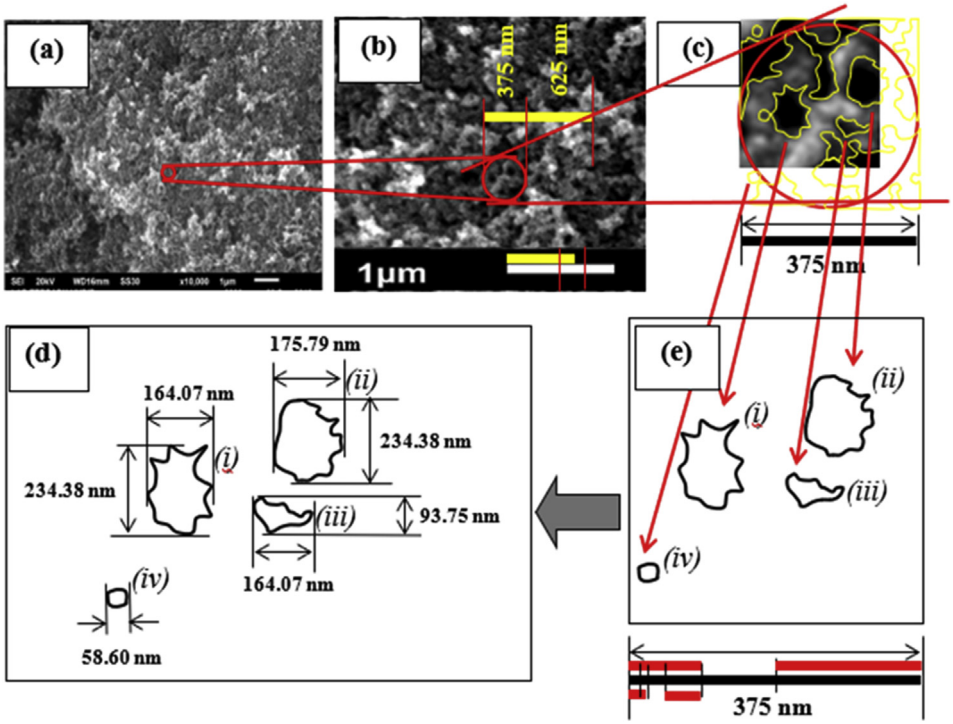

Figure 4. (a) SEM image of CBP materials surface morphology, 10,000 x magnification; (b) The 2 × 400% enlargement zoom of a localized CBP materials pores of SEM image; (c) Various forms of CBP materials pores obtained by 400% enlargement zoom of SEM image; (d) Sketched duplication of various forms of CBP materials pores surface including the pores sizes dimension; (e) Sketched duplication of various forms of CBP materials pores surface.

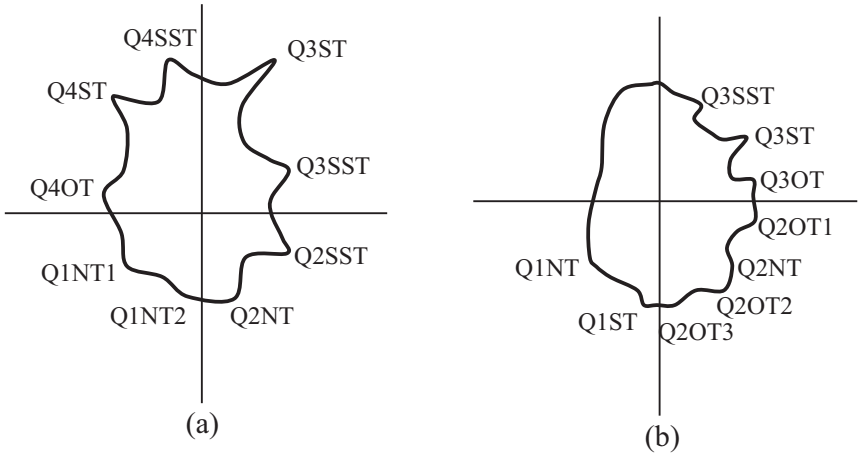

Figure 5. Enlarged pores of (a) mark *(i)*, and (b) mark *(ii)* shown in Figure 4d, e of CBP materials in which each completed by its specific turns name.

operated on the common used to explore the *d*-spacing of solid material using Cu anode material with K-Alpha1 wavelength of 1.541 Å; K-Alpha2 wavelength of 1.544 Å and K-Beta wavelength of 1.392 Å. The method in detail was adopted from Ungár et al. (2002).

2.2.4. Functional groups and chemical bonds analysis by FTIR spectrometer

Typical chemical bonds vibration and specific functional group of the ACBMPs materials molecular structure was confirmed by FTIR spectrometer (FTIR Perkin Elmer, USA) operated at default mode that commonly used to scan samples with PC based software controlled by instrument operation and data processing by referring to Yakout and El-Deen (2016). A small amount of ACBMPs materials were made into KBr pellets for FTIR analysis. The data of infrared transmittance was collected over a 4000 cm^{-1} to 500 cm^{-1} wave number range. All the samples were analyzed with KBr pellets as blank. The spectral data were compared with a reference to identify the functional groups and the covalent bonds vibration type existed in the sample.

2.2.5. The capability of adsorption test

The capability of adsorption test of the ACBMPs materials were performed towards methyl red (MR) solution of 1000 mg/L for 15 min contact time at room temperature and atmospheric pressure. Every 0.25 g of the fabricated ACBMPs was mixed with a fresh MR solution of 50 mL 1000 mg/L in a beaker glass and stirred at 200 rpm for 15 min with a magnetic stirrer. The mixtures were then centrifuged at 3000 rpm for 10 min and the MR solution of upper layer was separated from the associated ACBMPs adsorbent by filtration method using Whatman filtration paper. The quantity of MR before and after adsorption process

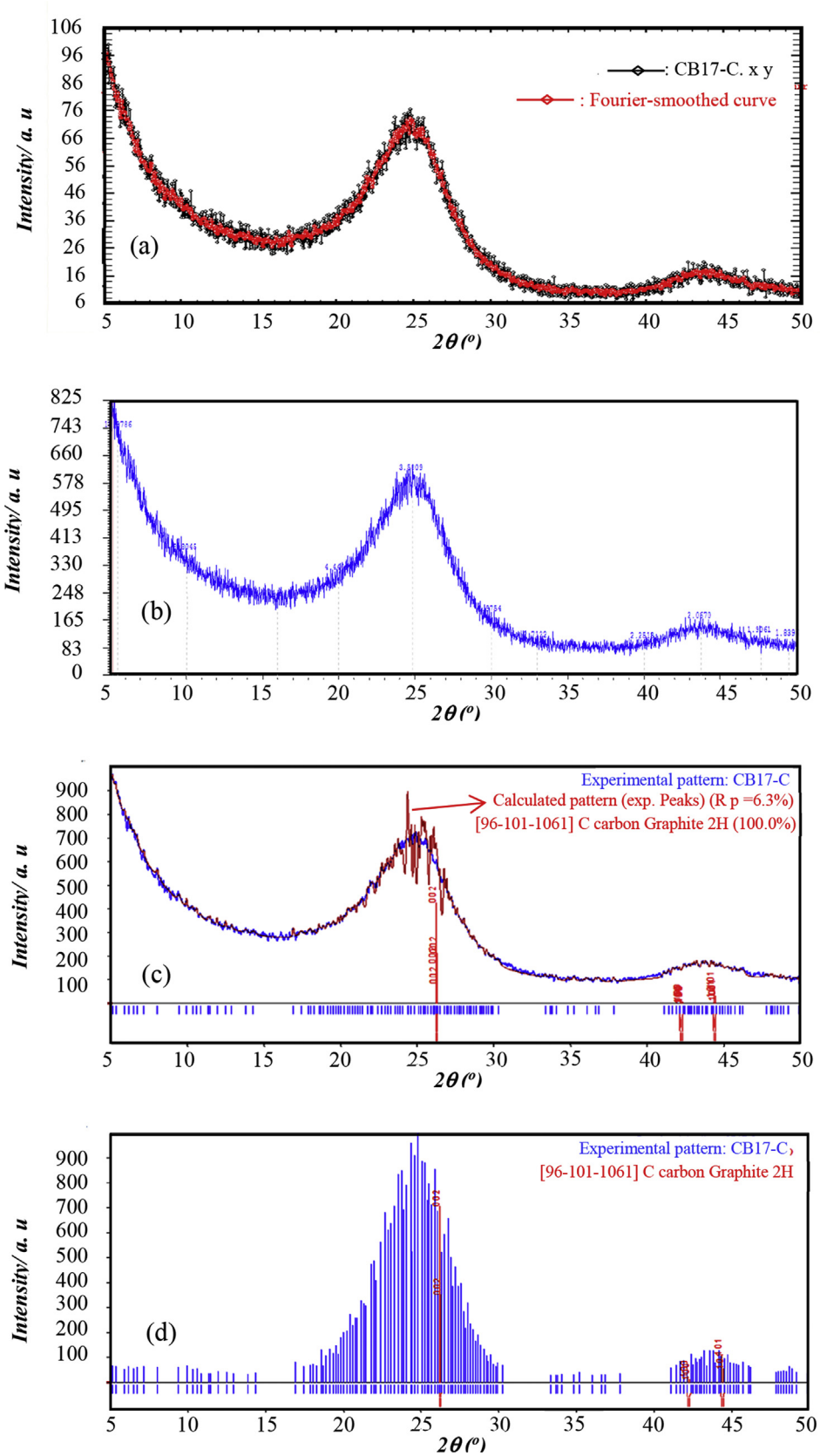

Figure 6. X-rays diffractogram of the fabricated ACBMPs materials, (a) Frontier smoothed curve of WinPLOTR analysis, (b) XPowder analysis, (c)–(d) Match! 3 analysis.

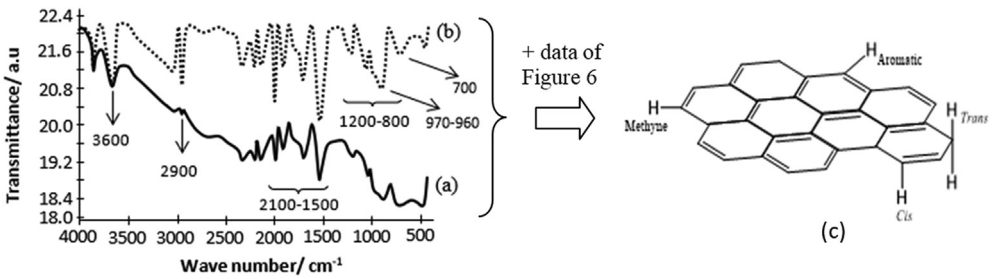

Figure 7. FTIR spectra of the fabricated ACBMPs materials, (a) Not normalized base line, (b) Duplication with normalized base line. (c) Result of the FTIR spectra interpretation, *i.e.* hypothetically structure of a graphene-like molecular sheet representative.

Table 1. The representatives' distance between parallel planes of atoms (d_{hkl}) of every value of 2θ of the fabricated ACBMPs materials molecular nanostructures main framework.

	1	2	3	4	5	6	7	8	9	10	11
$2\theta/^o$	5.53	10.04	15.99	19.98	24.84	30.01	33.00	40.02	43.76	47.67	49.51
d_{hkl}/Å	15.98	8.80	5.54	4.44	3.58	2.98	2.71	2.25	2.07	1.91	1.84
Intensity/100	86.8	42.4	24.2	34.9	71.2	19.9	10.3	9.8	17.2	12.2	11.0

was then determined by UV-Vis spectrometer at 522 nm maximum wavelength. The quantity of MR adsorbed was calculated according equation of $MR_{ads} = \{(MR_{initial} - MR_{final})$ where MR_{ads} is the quantity of MR adsorbed on the surface of ACBMPs materials, while $MR_{initial}$ and MR_{final} is MR concentration before and after adsorption process respectively. In this context, the quantity of MR concentration after adsorption was determined by using equation of $y = 0.0012x - 0.2443$ where y and x each is UV-Vis absorbance intensity of remaining MR and MR concentration in mg/L, the both were measured after adsorption process over.

3. Results and discussion

3.1. Particle size determination

The particles size analysis of the fabricated ACBMPs results are displayed in Figure 1. The Table of this Figure shows the statistical

Table 2. Summarized assignment of FTIR spectra displayed in Figure 7. The water molecules might be formed during the ACBMPs fabrication process at 400 °C for 60 min as the consequence of NaOH and H_3PO_4 reactions of activation process performed.

No.	FTIR spectra wave number/cm^{-1}	Atomic bonds vibration	References
1.	3600 (narrow)	Nonbonded hydrogen group, OH stretching	Coates (2019)
2.	2900	Methyne (=CH-) C–H stretching	Coates (2019)
		Methylene ($=CH_2$) C–H stretching	Coates (2019), Silverstein et al. (1981)
3.	2100–1500	Alkenyl C=C stretching	Coates (2019)
4.	1200–800	Skeletal C–C stretching	Coates (2019), Silverstein et al. (1981)
5.	970–960	*trans* C–H out-of-plane bend	Coates (2019)
6.	700 (broad)	*cis* C–H out-of-plane bend	Coates (2019)

Table 3. The quantity of MR adsorbed on the surface of ACBMPs materials fabricated on various temperature of 400, 500 and 600°C for various time of 20, 40 and 60 minutes each.

ACBMPs Materials									
Time	400 °C			500 °C			600 °C		
	Sample code	Remaining MR/(mg/L)	MR adsorbed/(mg/L)	Sample code	Remaining MR/(mg/L)	MR adsorbed/(mg/L)	Sample code	Remaining MR/(mg/L)	MR adsorbed/(mg/L)
	CBP*	663.000	337.000	CBP	663.000	337.000	CBP	663.000	337.000
20 mnt	CB13	673.889	**326.111**	CB110	427.778	572.222	CB119	416.111	583.889
	CB23	240.000	760.000	CB210	520.556	479.444	CB219	417.778	582.222
	CB33	372.222	627.778	CB310	356.667	643.333	CB319	365.556	634.444
40 mnt	CB14	214.444	785.556	CB113	347.778	652.222	CB122	306.111	693.889
	CB24	228.333	771.667	CB213	241.111	758.889	CB222	513.333	486.667
	CB34	302.778	697.222	CB313	385.000	615.000	CB322	500.556	499.444
60 mnt	CB17	86.667	**913.333**	CB116	270.556	729.444	CB125	164.444	835.556
	CB27	196.111	803.889	CB216	622.222	377.778	CB225	371.667	628.333
	CB37	185.000	815.000	CB316	462.778	537.222	CB325	530.000	470.000

Bold signifies the lowest quantity of MR adsorbed, and the highest quantity of MR adsorbed.

* CBP is CBOri that means an original activated carbon.

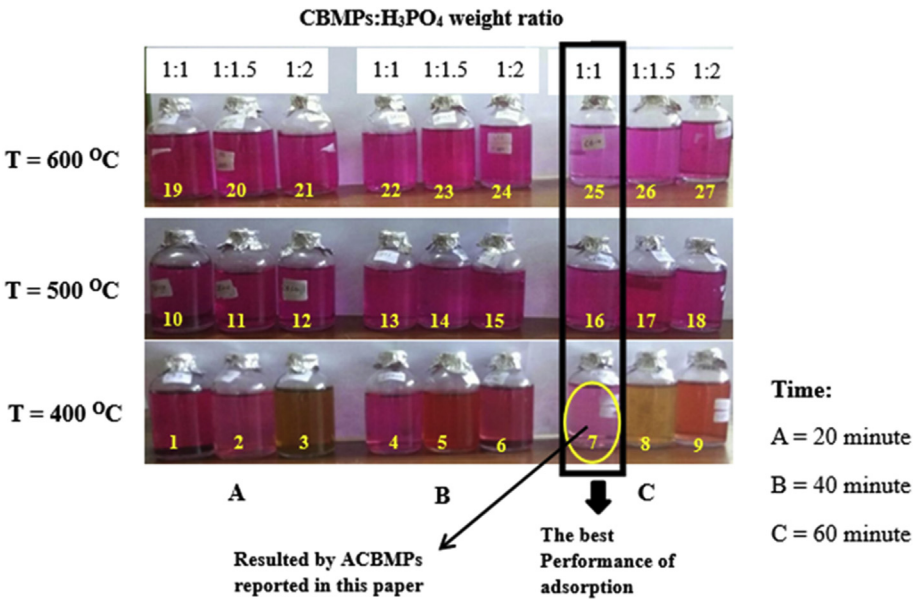

Figure 8. Photograph of the capability adsorption test of the ACBMPs materials for the removal of 1000 mg/L methyl red (MR) solution in original concentration. Adsorption process was performed for 15 min contact times. The first raw is color intensity of MR after adsorption, ACBMPs was activated by H_3PO_4 with weight ratio of 1:1; 1:1.5; 1:2 and heated at 600 °C for 20 min (column A), 40 min (column B) and 60 min (column C). The second raw is that heated at 500 °C for the same time as the first raw. The third raw is that heated at 400 °C for the same time as the first raw. Here, the Arabic number of 1 up to 27 each subsequently represents for sample encoded as CB13=>(1), CB23=>(2), CB33=>(3), CB14=>(4), CB24=>(5), CB34=>(6), CB17=>(7), CB27=>(8), CB37=>(9), CB110=>(10), CB210=>(11), CB310=>(12), CB113=>(13), CB213=>(14), CB313=>(15), CB116=>(16), CB216=>(17), CB316=>(18), CB119=>(19), CB219=>(20), CB319=>(21), CB122=>(22), CB222=>(23), CB322=>(24), CB125=>(25), CB225=>(26) and CB325=>(27).

calculation of the generated curve pattern of the particles size distribution of the ACBMPs material. It can be seen that a mean diameter of 1219.6 nm (~1.2 μm) in size with standard deviation (SD) of 453.0 nm (~0.5 μm), mode of 1132.0 nm (~1.1 μm), Z-average of 1459.6 nm (~1.5 nm) and poly dispersion index (PI) of 0.531. It indicated that the ACBMPs particles populations are about from 766.6 nm (0.8 μm) up to 1672.6 nm (1.7 μm) in size.

Of the aforementioned population, about 75% of the particles belong to undersize of mean, *i.e.* 1219.6 nm with the most frequent detected was the particles of 1132 nm in size. The undersize percentage of ACBMPs is in accordance with its poly dispersion (PI) index of which is 0.531. However, regarding the smaller the particles will be the better the properties of the surface area, and then the fabricated ACBMPs was further characterized.

3.2. Surface morphology

The surface morphology of the fabricated ACBMPs has been investigated by SEM and the images are presented in Figure 2. This figure shows that ACBMPs particles have various sizes ranging from 100 nm up to 1.85 μm in diameter and being assembled randomly and constructed the throughout fabricated ACBMPs materials.

Surprisingly, almost all the particles tend to form particles clusters rather than an individual particle of which among of them were marked by Arabic numbers of 1, 2, 3, 4, 5 and 6. This situation fits with the data of particles size analysis (PSA) of the associated ACBMPs materials shown in Figure 1 that provide confirmation of the ACBMPs particles were about ranging from 766.6 nm (0.8 μm) up to 1672.6 nm (1.7 μm) in size. Despite the ACBMPs particles of less than 766.6 nm (0.8 μm) in size were not detected by a PSA machine at all, but they can be clearly detected by SEM as shown in Figure 2. Focusing our attention on about 500 nm ACBMPs particles of marked 2 shown in Figure 2a–c, e, f as a representative of the fabricated ACBMPs particle, it is very clear that the ACBMPs belongs to various forms of pores with different sizes and depths. In this case, the darker the pores images the deeper the associated pores and vice versa so that the pores can be imagined as a lake or sea of nano-scale in size. Moreover, the several pores images can be enlarged as shown in Figure 2d, e and we can observe so many turns and basins were generated randomly on the associated pores. These facts demonstrate that sp^3 and sp^2 hybrids orbitals of carbon-carbon bond thoroughly constructed the fabricated ACBMPs materials molecules play important role in the formation of the turns and basin. In this relation, it has widely known that any material including carbon-based materials such as ACBMPs is basically constructed by certain molecules, and in this context by solid hydrocarbon molecules framework. Hydrocarbon molecules are built by carbon-carbon atoms covalent bonds of which dominated by sp^3 and sp^2 hybrids orbitals (Armano and Agnello, 2019; Sreeprasad and Berry, 2013; Peschel, 2011) for forming very dense-compact molecular structure. It leads the physical and chemical properties, even surface morphology of any materials, including ACBMPs materials are essentially determined by the molecules structure constructed them, configuration, chemical bonds, atomic bond angles and plane shape of the associated molecule. In relation with activated carbon-based materials, so many references reported that this material is throughout constructed by graphene-like sheets or graphitic-like molecular structures (Yang et al., 2019; Nagornaya et al., 2016; Harris et al., 2008). This conclusion was supported convincingly by both its spectra of infrared spectroscopy and diffractogram of X-ray diffraction patterns. It is similar to which resulted by our research as shown in Figures 6 and 7. In this relation, sp^3 and sp^2 hybrids orbital of carbon atoms constructed the covalent bonds of the graphene-like sheets or graphitic-like molecular structures form tetrahedral and trigonal planar monohedral respectively. As the consequence of this situation is many turns or basin generated on the surface of any activated carbon-based materials particles including this ACBMPs produced in this research. The turns and basins are generated by carbon-carbon-carbon bonds sp^3 and sp^2 hybridizations having about

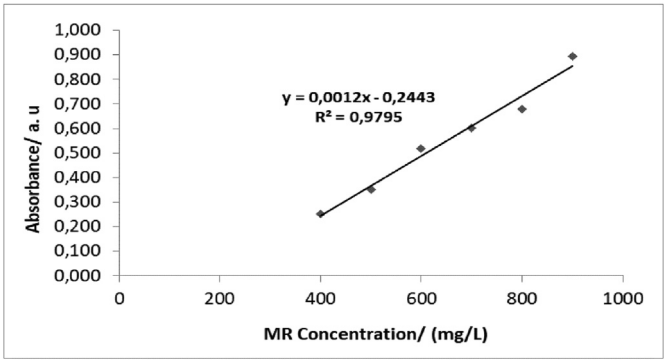

Figure 9. Standard curve of methyl red (MR) solution correlated between. the MR concentration in mg/L unit versus its UV-Vis absorbansce at 522 nm maximum wavelength.

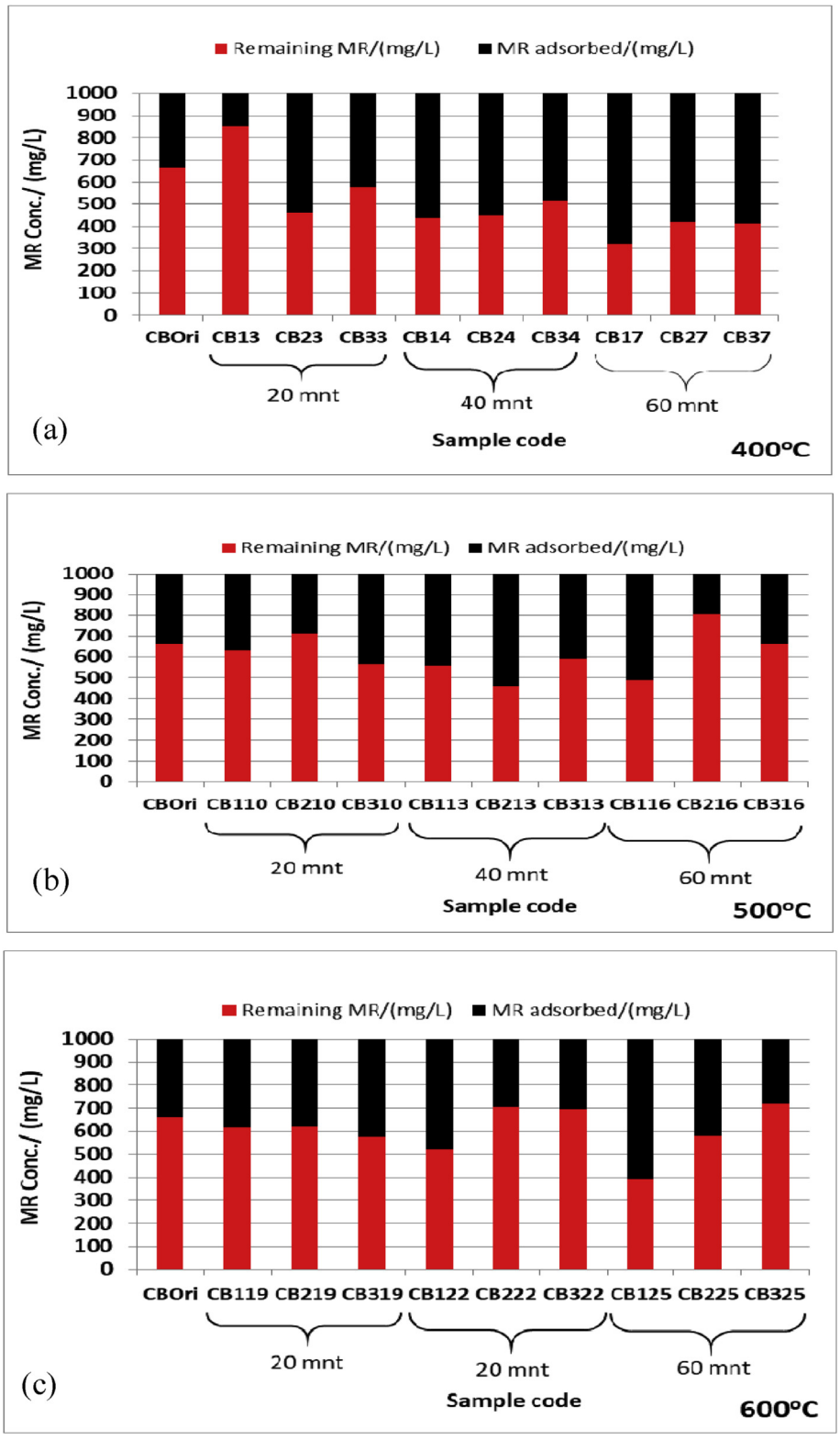

Figure 10. A graph of the remaining and adsorbed methyl red (MR) according to the calculation displayed in Table 3, (a) sampel of ACBMPs_CB13 up to ACBMPs_CB37; (b) ACBMPs_CB110 up to ACBMPs_CB316; (c) ACBMPs_CB119 up to ACBMPs_CB325.

99−109° and 115−120° bonds angles with carbon-carbon bond length of approximately about 1.54 Å (0.154 nm) and carbon-hydrogen bonds length of approximately about 1.05Å (0.105 nm) respectively (Cotton et al., 1995). Thus, when the individual carbon-based particles with certain quantity were deposited on a solid support material, they doing self-assemble each other and many voids will be generated among the particles. In this situation, such turns and basins can act as harbours-like nano structure for various guest molecules to temporary transit before entering into the associated particles body. The long-time the molecules stay in the harbours would be depended on the size and shape of the angles which construct collectively the associated harbours. It means that there is very important relation between size as well as shape of the

angles of the particles body (in one side) and molecular kinetics mechanism (in other side) during adsorption, absorption as well as desorption processes going on. In addition, the sp^3 hybridization of carbon-carbon covalent bonds are capable not only to rotate around its associated axes but also to bend and they are very responsive toward thermal energy change hit them. As shown in Figures 2 and 4, scanning electron microscope (SEM) images of the surface morphology of the carbon-based particles provide clearly the size and shape of the angles of which form specific surface morphology that can be explored through several times magnification method of the associated SEM images.

In this case, some specific binding sites as well as active sites are probable located on the turns of the pores building. The binding sites will take a role to bind molecules that already adsorbed selectively whereas the active sites will catalyze the adsorbed molecules during reactions progress when the counterpart molecules also present in the pores. Accordingly, a pore that has the more turns will also has the more binding sites and the consequence is the pores will have higher capacity of adsorption compared to the less ones. For examples, pores of mark *(i), (ii) and (iii)* shown in Figure 2c, f have 11, 19 and 16 turns respectively, so pore of mark *(ii)* will has the highest adsorption capacity subsequently followed by that of *(iii)* and *(i)*. It is a coincident if a pore of mark *(ii)* is also the biggest in turn based on size and that of *(i)* is the smallest one.

In this relation, we classify a significant angle formed in the pore surface becomes four groups of angles of turns adopting the terminology of quadrant that commonly applied in a mathematical science. Based on this terminology, one can divide each pore into four parts so that the angles of turns can also be classified becomes four groups. Those are, the first is a group of turns that has θ angles of the first quadrant of $0^o - 90^o$ range in radian unit. The second one, the third one and the fourth one each is that of the second, the third and the fourth quadrant angles of $90^o - 180^o$, $180^o - 270^o$ and $270^o - 360^o$ ranges respectively. In addition, one can also divide the angles of turns aforementioned further becomes four categories depending on the value of θ angle range, the first one is the sharp turns that have θ angles of $0^o - 30^o$, $90^o - 120^o$, $180^o - 210^o$ or $270^o - 300^o$ ranges. The second one is the semi sharp turns that have θ angles of $30^o - 60^o$, $120^o - 150^o$, $210^o - 240^o$ or $300^o - 330^o$ ranges, the third one is the obtuse turns that have θ angles of $60^o - 90^o$, $150^o - 180^o$, $240^o - 270^o$ or $330^o - 360^o$ ranges, and the forth one is the turns formed angles of more than 90^o, 180^o, 270^o or 360^o can be categorized as non-significant angles. Accordingly, it can be proposed a new nomenclature of typical turns commonly generated in pores surface of carbon black-based materials in particular based on both quadrants and radian angles terminologies. A guidance of the turn's nomenclature of carbon black-based pore surface aforementioned is then drafted in Figure 3. Figure 3a shows a pore surface depicted in Figure 2c, f mark *(iii)* in a larger scale as a representative pore that has been divided into four parts by putting a (x-y) coordinate on its surface, and (b) a map of quadrant-based angles in radian unit as a tool to name the associated turns of the pore surface. Based on the map, the direction of turns forming θ_1, θ_2, θ_3, θ_4 and θ_5 angles are similar to the angles of the third quadrant (Q3). However, in particular magnitude of the angles mentioned are approximately in $180^o - 210^o$ range for θ_1, namely sharp turn, in contrast the other angles of θ_2, θ_3, θ_4 and θ_5 each is more than 270^o, namely non-significant turns.

Thus, the turn of θ_1 can be named as Q3ST1 where ST stands for sharp turn, whereas θ_2, θ_3, θ_4 and θ_5 can be named as Q3NT2, Q3NT3, Q3NT4 and Q3NT5 respectively where NT stands for non-significant turn. Moreover, with similar manner as above, the turns formed angles of θ_6 and θ_7 can be named as Q4OT6 and Q4OT7 respectively, where OT stands for obtuse turn. It is also, the turns formed angles of θ_8, θ_9, θ_{10}, θ_{11} can be named as Q1OT8, Q1NT9, Q2NT10 and Q2NT11 respectively. However semi sharp turns were not generated in the pore surface of mark *(iii)* showed in Figure 2c, f in all the quadrants given.

On the other hand, we define the size of the pores surface is the longest distance between its two opposite sides, for instance the pore surface of *(i)*, Figure 2c is approximately about 156.25 nm × 125 nm in size with the sharp turn Q3ST of 62.5 nm depths. The pore surface of mark *(ii)* is approximately about 375 nm × 281.25 nm in size without significant turns in all the quadrants. The pore surface of mark *(iii)*, Figure 2c is approximately about 281.25 nm × 162.25 nm in size with the sharp turn Q3ST1 of 156.25 nm depths. However, the size of pore will have correlation with adsorption capacity to load the adsorbate molecules of which the bigger the pore the higher the adsorption capacity. In contrast, the sharpness of turns will have correlation with the capability of binding sites to keep selectively the adsorbed molecules stay in the pores after adsorption process. In this case, the sharper the turns the longer the molecules adsorbed stay in the associated pores. Furthermore, as a comparison, we can look surface morphology of pristine carbon black (CBP) explored with the same SEM shown in Figure 4. Figure 4 shows typical pores generated on a bulk CBP that little bit different from the pores generated on ACBMPs materials. Any interesting particles clusters are not generated on the bulk CBP materials.

As an evidence, a small area of about 375 nm contains 10 pores with various shape and size can be seen in Figure 4c. However similar turns as happened in ACBMPs materials pores are also generated in the bulk CBP materials with lesser amount of turns per pore.

In this relation, we can see Figure 4d, e, several pores of bulk CBP materials have been sketching manually in this figure based on their SEM images of Figure 3a–c. Here, the pore surface of mark *(i), (ii), (iii)* and *(iv)* belongs to 17, 14, 9 and no turns respectively. The size of the surface can also be determined approximately based on the barcode given of which is about 234.38 nm × 164.07nm, 234.38 nm × 175.79 nm, 164.07 nm × 93.75 nm and 58.60 nm for that of mark *(i), (ii), (iii)* and *(iv)* respectively.

Nevertheless, the turns formed on the pores surface of CBP materials are similar in shape and pattern with that of the fabricated ACBMPs20_x materials. It leads to the nomenclature of turns generated in the pore surface proposed above can also be applied to name the CBP pores surface shown in Figure 4a–e. Accordingly, a pore of mark *(i)* is about 164.07 nm × 234.38 nm in size with many specific turns of Q1NT1, Q1NT2, Q2NT, Q2SST, Q3SST, Q3ST, Q4SST, Q4ST and Q4OT. While, a pore of mark *(ii)* is about 175.79 nm × 234.38 nm in size with specific turns of Q1NT, Q1ST, Q2OT1, Q2OT2, Q2OT3, Q2NT, Q3OT, Q3ST and Q3SST. The both typical pores of CBP completed with the name of the associated turns are depicted in Figure 5. The presence of the turns probable had accommodate the hysteresis adsorption phenomenon occurred during nitrogen gas adsorption-desorption test was performed.

3.3. The parallel planes distance (d-spacing) analysis by XRD spectroscopy

X-ray diffractogram of the fabricated ACBMPs materials is depicted in Figure 6. Using a WinPLOTR graphic tool for powder diffraction of version 2010, XPowder ver.2004 and Match!3 software we analyze the diffractogram in detail. The diffractograms pattern shown by Figure 6a confirmed clearly typical nanostructures of the fabricated ACBMPs materials comprised of three atomic planes clusters. The first cluster provided 2θ X-ray diffractogram of around $5^o - 10^o$ ranges with maximum intensity of around 96 a.u, the second one provided that of around $20^o - 30^o$ ranges with maximum intensity of around 76 a.u and the third one provided that of around $40^o - 50^o$ ranges with maximum intensity of around 16 a.u.

The intensity of the diffractogram peaks represents the relative amount of the atomic clusters where the higher the intensity the more amount of the atoms. In correlation to that, it has been well known that each value of 2θ represents the distance between parallel planes of atoms (d_{hkl}) in the family of *hkl* Miller indexes of the associated materials as stated by Bragg's law, $d_{hkl} = \lambda/2\mathrm{Sin}\theta$. In this relation, by using XPowder ver.2004 software we analyzed the diffractogram to determine the d_{hkl} of every value of 2θ, and the result is displayed in Figure 7b. This figure shows d_{hkl} of the first atomic cluster of 2θ about $5.53^o - 10.04^o$ range is 15.98 angstrom (Å) up to 8.80 Å, d_{hkl} of the second atomic cluster of 2θ

about 19.98° – 30.01° is 4.44 Å up to 2.98 Å, and d_{hkl} of the third atomic cluster of 2θ about 40.02° – 30.01° is 2.25 Å up to 1.91 Å. These facts attributed the distance between parallel planes of atoms built the molecular nanostructures main framework of the fabricated ACBMPs materials are quite varies in distance from the longest of around 15.98 Å to the shorter of around 1.91 Å.

This situation leads to the intraparticles microporous nanostructures connected each other were formed properly with various shapes and sizes. In addition, more complete d_{hkl} of every value of 2θ of the fabricated ACBMPs materials molecular nanostructures main framework shown in Figure 6b is displayed in Table 1.

Unfortunately, the existence of the intraparticle micropores in respective of their shape and size cannot be investigated by using SEM. However, it can be well understood that the fabricated ACBMPs materials belong to two kinds of pores of which the first one is interparticle pores that have bigger in size as shown in Figures 2 and 4. The second one is intraparticles pores that have much smaller in size. Referring Wibawa et al. (2011) the interparticle pores can be named as secondary pores, and the intraparticles pore can be named as primary pores.

Furthermore, Figure 6c and d provide the evidence of many various distance between parallel planes of atoms constructed the fabricated ACBMPs materials. It can be seen clearly that the distances can be resolved properly becomes three clusters of lines diffractogram instead of board one in which the densest population of atoms are located at 2θ of around 20°–30° range and subsequently followed by that of around 43°–47° and 5°–15° ranges. In addition, fitting to the available database already installed in the associated devices it is well known that molecular structure of the fabricated ACBMPs materials framework is similar to carbon graphite of 2H hardness as stated in the legend of Figure 6c and d with the vast majority of carbon atomic plane is 002 and 101 family.

3.4. FTIR spectroscopy analysis

The FTIR spectrum of the fabricated ACBMPs materials is depicted in Figure 7. This Figure shows the ACBMPs particles generated six particular FTIR spectra wavenumber peaks of 3600 cm^{-1}, 2900 cm^{-1}, 2100–1500 cm^{-1}, 1200–800 cm^{-1}, 970−860 cm^{-1}, and 700 cm^{-1} which can be interpreted clearly according to the references given (Coates, 2019; Silverstein et al., 1981). These spectra attributed that molecular framework constructed the fabricated ACBMPs material belongs to several functional groups. Those are water molecules that might be trapped in the suitable pores of the associated material or in interlayer graphene-like structure sheets as narrow wave number peak of around 3600 cm^{-1} appeared that presenting nonbonded O–H stretching vibration (Coates, 2019). The others are methyne (=CH-), methylene ($=CH_2$), alkenyl C=C, skeletal C–C, vinylidene C–H out-of-plane bend, *trans* C–H out-of-plane bend and *cis* C–H out-of-plane bend (Coates, 2019; Silverstein et al., 1981). Complete assignment of the FTIR spectra peaks displayed in Figure 7 is summarized in Table 2. These atomic bonds' vibration aforementioned confirmed that graphene-like molecular structures is the main construction of the fabricated ACBMPs material. This structure is quite match to the XRD analyses described in section 3.3 of which provide confirmation that carbon graphite is a main molecular structure thoroughly constructed the materials.

3.5. The capability of adsorption

As mentioned in above description that surface morphology pattern of any carbon-based material, including ACBMPs produced in this research is basically constructed by many turns and basins resulted by sp^3 and sp^2 carbon-carbon bonds hybridizations collectively. The effect of the turns and basins towards adsorption properties of the ACBMPs materials were evaluated towards methyl red (MR) solution of 1000 ppm concentration, and the result is displayed in Table 3. Table 3 shows capability of adsorption of various ACBMPs materials to remove MR molecules from its associated solution were very varied from the least, 326.111 mg/L performed by ACBMPs of CB13 code to the highest, 913.333 mg/L performed by ACBMPs of CB17 code. These facts demonstrate that temperatures of which represent the quantity of thermal energy and duration heating during fabrication process of ACBMPs materials are very important factors influencing the capability of adsorption of the associated ACBMPs materials. It proofs that thermal energy hit the materials leads the carbon-carbon-carbon bonds of sp^3 hybridizations rotate around axes and bend to reach the best position of stability. When this case happened on the surface of ACBMPs materials, it generates surface morphology with various turns and basins. The much more turns and basin the higher the capability of adsorption of the ACBMPs materials due to the associated turns and basin will be temporary places for MR molecules to stay before they enter into the particles body of the ACBMPs materials, and vice versa.

In relation to those, the color degradations of methyl red (MR) due to adsorption process on the surface of the ACBMPs materials fabricated at various thermal energy exposure for various times, in which the quantity in mg/L unit displayed in Table 3, are shown in Figure 8.

Figure 8 shows that the T = 400 °C row, column C in particularly marked 7 provides the lowest MR color in intensity as it is the most brightness orange compared the others ones. In contrast, the T = 400 °C row, column A in particularly marked 1 provides the highest MR color in intensity since it is the darkest orange than the others ones. The various color intensity demonstrated the capability of adsorption of the various ACBMPs are quite different each other due to the turns and basins generated on the outer surface of the ACBMPs individual particles are also different in shape and size. This fact proofs that the turns and basins aforementioned have successful played their role as places to temporary stay the MR molecules before entering into the ACBMPs particles body.

On the other hand, the dark brown and bright brown color of the remaining MR shown in mark 3 and 8 respectively might indicate the catalytic degradation of the MR molecules happened rather than adsorption process. This phenomenon could happen since the turns and basins generated on the outer surface of ACBMPs_CB33 and ACBMPs_CB316 are quite specific and so differ compared to that generated on that of ACBMPs_CB17 as well as the others.

Furthermore, as stated in sub section 2.2.5 above, a simple linear equation of $y = 0.0012x - 0.2443$ with the best coefficient correlation, R^2 of 0.9795 had been applied to convert the MR color intensities shown in Figure 8 from their absorbance values of the UV-Vis lights beamed to the MR solution become mg/L in concentration unit. In this context, the common Microsoft Excel software had been used to firstly established the standard curve show in Figure 9.

Due to so very important the role of the turns and basins in adsorption and catalytic degradation process of any guest molecules, in this case is MR molecules, on the surface of the ACBMPs materials, it is necessary to make someone can easier to catch and interpret proper quickly the difference of the capability of adsorption of the ACBMPs materials, then data in Table 3 can also be shown as a graph such as displayed in Figure 10.

Now we can interpret just by looking glanc at Figure 10 that ACBMPs_CB17 material provides the highest capability of adsorbption for removing MR molecules as the black part of the associated graph of which represented the adsorbed MR, is the longest compared to the others. In contrast, we can also look glancy at the same Figure that ACBMPs_CB13 material provides the lowest capability of the adsorption for the same molecules as the red part of the associated graph is the shortest than the others.

4. Conclusion

The activated carbon black (ACB)–based materials of ACBMPs is a porous material constructed by graphene-like structure lying sheets with distance between the sheets were quite vary ranging from approximately around 1.84 Å up to 15.98 Å. The distances formed intraparticle pores with various shapes, size and orientation of which interconnecting each

other. On the other hand, very unique interparticles pores (voids) of about 150 nm up to 400 nm in average diameter in which many various turns formed on inside the pores wall. The turns play a role of binding sites or active sites for the guest molecules enter into the pores. Based on the directions, the turns can be categorized into four categories, *i.e.* quadrant one (Q1), two (Q2), three (Q3) and four (Q4) is proposed. While that, based on the shapes, the turns can be classified also into four classes, *i.e.* sharp, semi sharp, obtuse and non-significant turns depending on the angle of the associated turn in radian angle, θ. The voids with more sharp turns will have more binding or active side so that more molecules in quantity can be bound into the pore and vice versa. Accordingly, the new nomenclature method of interparticles pores can be proposed based on both parameters the direction of the pores and the shapes ones. Last but not least, the combination of ultrasonic and thermal energy treatments in fabricating ACBMPs could generate binding or active site points with unique shapes as a transit terminal for any guest molecules.

Declarations

Author contribution statement

Pratama Jujur Wibawa: Conceived and designed the experiments; Performed the experiments; Analyzed and interpreted the data; Contributed reagents, materials, analysis tools or data; Wrote the paper.

Muhammad Nur, Hadi Nur: Analyzed and interpreted the data.

Mukhammad Asy'ari: Contributed reagents, materials, analysis tools or data.

Funding statement

This work was supported by Diponegoro University through an International Publication Research grand schema with the PNBP DIPA budgeting source of number SP DIPA–042.01.2.400898/2016, December 7, 2015 fiscal year 2016.

Competing interest statement

The authors declare no conflict of interest.

Additional information

No additional information is available for this paper.

Acknowledgements

The authors are grateful for the financial support from Diponegoro University through an International Publication Research grand schema with the PNBP DIPA budgeting source of number SP DIPA–042.01.2.400898/2016, December 7, 2015 fiscal year 2016.

References

Armano, A., Agnello, S., 2019. Two-dimensional carbon: a review of synthesis methods, and electronic, optical, and vibrational properties of single-layer graphene. J. Carbon Res. 5 (67), 1–37.

Coates, J., 2019. In: Meyers, R.A. (Ed.), Interpretation of Infrared Spectra, A Practical Approach, Encyclopedia of Analytical Chemistry. Copyrights John Wiley & Sons Ltd, pp. 1–23. http://www3.uma.pt/jrodrigues/disciplinas/QINO-II/Teorica/IR.pdf. Online accessed on Wednesday, August 28, 2019 at 08.00 a.m. Indonesian western time.

Cotton, F.A., Wilkinson, G., Gaus, P.L., 1995. Basic Inorganic Chemistry, 3rd. Edition. John Wiley & Sons, New York, pp. 87–88. 97.

Gratuito, M.K.B., Panyathanmaporn, T., Chumnanklang, R.A., Sirinuntawittaya, N., Dutta, A., 2008. Production of activated carbon from coconut shell: optimization using response surface methodology. Bioresour. Technol. 99, 4887–4895.

Hallett, F.R., 1994. Particle size analysis by dynamic light scattering. Food Res. Int. 27 (2), 195–198.

Horiba, 2014. Scientific Guide Book Particles Size Analysis. Horiba Instrument Inc, 9755 Research Drive, Irvine, CA 92618 USA, 1-800-4-Horiba. www.horiba.com/us/particle.

Harris, P.J.F., Liu, Z., Suenaga, K., 2008. Imaging the atomic structure of activated carbon. J. Phys. Condens. Matter 20, 1–5, 36220.

Jutakridsada, P., Prajaksud, C., Aruk, L.K.-, Theerakulpisut, S., Kamwilaisak, K., 2016. Adsorption characteristics of activated carbon prepared from spent ground coffee. Clean Technol. Environ. Policy 18, 639–645.

Mailer, A.G., Clegg, P.S., Pusey P, N., 2015. Particle sizing by dynamic light scattering: non-linear cumulant analysis. J. Phys. Condens. Matter 27 (14), 145102.

Nagornaya, M.N., Razdyakonova, G.I., Khodakova, S.Y., 2016. The effect of functional groups of carbon black on rubber properties: International Conference on Oil and Gas Engineering. Procedia Eng. 152, 563–569.

Nallusamy, S., Saravanan, S., Kannarasu, V., Narayanan, M.R., 2017a. Experimental analysis on reinforced aluminium metal matrix with boron carbide, graphite and fly ash chemical composites. Ras?yan J. Chem. 10 (4), 1368–1373 pISSN: 0974-1496, eISSN: 0976-0083.

Nallusamy, S., Narayanan, M.R., Logeshwaran, J., 2017b. Synthesis and machining characterization of copper-multiwalled carbon nanotubes-graphene hybrid composite using SEM and ANOVA. J. Nano Res. 50, 105–115.

Nallusamy, S., 2016. A Review on the effects of casting quality, microstructure and mechanical properties of cast Al-Si-0.3Mg alloy. Int. J. Perform. Eng. 12 (2), 143–154.

Narayanan, M.R., Nallusamy, S., Kumar, S.L., 2018. Characterization of machining paramaters on EN31 with Al2O3 Nanoparticles using Taguchi technique. Int. J. Mech. Eng. Technol. 9 (1), 1173–1183 pISSN: 0976-6340, eISSN: 0976-6359.

Peschel, G., 2011. Carbon-carbon Bonds: Hybridization. http://www.physik.fu-berlin.de/einrichtungen/ag/ag-reich/lehre/Archiv/ss2011/docs/Gina_Peschel-Handout.pdf. down-loaded: Saturday, February 2, 2020 at 02.00 p. m Western Indonesian Time.

Sairanen, E., 2015. Modification of Carbon Materials for Catalyst Applications. Unigrafia Oy, Helsinki, 2015, Aalto University publication series, Doctoral Dissertations 21/2015. Aalto University, P.O. Box 11000, FI-00076 Aalto. www.aalto.fi. http://urn.fi/URN.

Shafeeyan, M.S., Wan Daud, W.M.A., Houshmand, A., Shamiri, A., 2010. A review onsurface modification of activated carbon for carbon dioxide adsorption. J. Anal. Appl. Pyrol. 89, 143–151.

Show, Y., Ueno, Y., 2017. formation of platinum catalyst on carbon black using an in-liquid plasma method for fuel cells. Nanomaterials 7 (31), 1–9.

Silverstein, R.M., Bassler, G.C., Morril, T.C., 1981. Spectrometric Identification of Organic Compounds, 4th. Edition. John Wiley & Sons, New York.

Sreeprasad, T.S., Berry, V., 2013. How do the electrical properties of graphene change with its functionalization? Small 9 (3), 341–350.

Suhas, Carrott, P.J.M., Carrott, M.M.L.R., 2007. Lignin – from natural adsorbent to activated carbon: a review. Bioresour. Technol. 98, 2301–2312.

Suryanto, B.H.R., Zhao, C., 2016. Surface-oxidized carbon black as a catalyst for the water oxidation and alcohol oxidation reactions. Chem. Commun. 52, 6439–6442.

Ungár, T., Gubicza, J., Ribárik, G., Pantea, C., Zerda, T.W., 2002. Microstructure of carbon blacks determined by X-ray diffraction profile analysis. Carbon 40, 929–937. PII: S0008-6223(01)00224-X.

Veksha, A., Bhuiyan, T.I., Hill, J.M., 2016. Activation of aspen wood with carbon dioxide and phosphoric acid for removal of total organic carbon from oil sands produced water: increasing the yield with bio-oil recycling. Materials 9, 20.

Wibawa, P.J., Saim, H., Agam, M.A., Nur, H., 2011. Design, preparation and characterization of polystyrene nanospheres based–porous structure towards UV–vis and infrared light absorption. Phys. Procedia 22, 524–531.

Yakout, S.M., El-Deen, G.S., 2016. Characterization of activated carbon prepared by phosphoric acid activation of olive stones. Arab. J. Chem. 9, S1155–S1162.

Yang, X., Wan, Y., Zheng, Y., He, F., Yu, Z., Huang, J., Wang, H., Ok, Y.S., Jiang, Y., Gao, B., 2019. Surface functional groups of carbon-based adsorbents and their roles in the removal of heavy metals from aqueous solutions: a critical review. Chem. Eng. J. 366, 608–621.